Miniature Shock Tube Actuators for High Speed Flow Control Applications

Rakesh Chandran Ramachandran[1], and Ganesh Raman[2]
Mechanical, Materials and Aerospace Engineering Department, Illinois Institute of Technology, 10 W 32nd Street, Suite 243, Chicago, IL 60616, USA

Received date 24th September 2012; Accepted date 27th January 2013

Abstract
There is a critical need to develop reliable high control authority flow control actuators for high speed applications. This paper introduces a novel high control authority actuator in the form of a miniature shock tube actuator. Two types of shock tubes were developed, namely, a single driver and a multiple driver shock tube. Various characterization experiments performed on these shock tubes revealed that they produced high intensity shock waves as predicted by one dimensional shock wave theory. The actuators were then tested for their effectiveness in suppressing cavity noise. The flow control experiments revealed that the shock tubes produced a 12 dB and 10 dB suppression in tonal noise for Mach numbers of 0.6 and 0.8, respectively. These results were compared to a fast acting solenoid valve providing steady and pulsating mass injection. Details of the flow field being controlled were studied using mean velocity and phase averaged measurements. With further development such actuators have potential for use in high speed flow control situations.

1. INTRODUCTION

In the field of aeroacoustics, one of the primary areas of interest has been resonant flows. Fluid structure interactions gives rise to a reverberant field, which results in high amplitude fluctuating pressures associated with the resonant tones that could lead to sonic fatigue failure of sensitive components in the vicinity of such flows. One such resonant interaction is the cavity flow problem. Several flow control technologies exist to suppress cavity tones but most of them lose efficacy at off-design conditions and particularly at higher subsonic and supersonic flows. It is due to this fact that there is a high demand for high control authority flow control actuators. In order for an actuator to have higher control authority, one must use a mechanism that has sufficient energy to disrupt the cavity tone generation mechanism at higher subsonic Mach numbers. One such mechanism is the shock tube that generates high strength shock waves. To the best of our knowledge([1], [2])there does not appear to be any use of shock waves to suppress noise emitted by cavities in aircraft. The mechanism of cavity noise generation and the theory behind shock tubes are discussed next.

1.1 Cavity Flows

Cavity flow resonance occurs when free stream air flows over an open cavity. These kind of scenarios can be observed in a variety of practical situations. The more prominent ones are observed in aerospace applications such as flows over open weapon bays and landing gear wells. Some other examples include air flowing over an open sun-roof of a car. Under certain conditions these flows produce intense acoustic tones, also known as the cavity tones, at discrete frequencies. These acoustic tones are also accompanied by both pressure and velocity fluctuations which could affect the structure of the aircraft or vehicle and cause damage to the instrumentation stored. In this section we will discuss the physical mechanism behind the generation and prediction of cavity tones, their classification and a brief background on the various studies conducted on this topic.

The mechanism of cavity tone production falls under the category of the resonant acoustic production mechanisms. Among them are the mechanisms which give rise to screech tones [3], jet impingement tones [4], edge tones [5] and ring tones [6]. All these phenomenon rely on a feedback loop

[1]Graduate student, Email: rramac4@hawk.iit.edu

[2]Deputy Vice-Provost for Research, Email: raman@iit.edu

comprising of impingement of the unstable shear layer and upstream propagating acoustic waves.

When a free stream of air flows over a cavity a shear layer is formed due to the velocity difference between the free stream flow and the slower moving flow within the cavity. The instabilities in the free shear layer amplify as they propagate downstream before finally arriving at the downstream edge of the cavity. Upon hitting the downstream edge, the instabilities give rise to acoustic waves that propagate upstream and further excite the newly formed disturbances at the upstream edge of the cavity, thereby completing the feedback loop. This feedback loop gives rise to intense acoustic tones at discrete frequencies, known as cavity tones. A schematic of the feedback loop mechanism in the cavity is shown in figure 1.

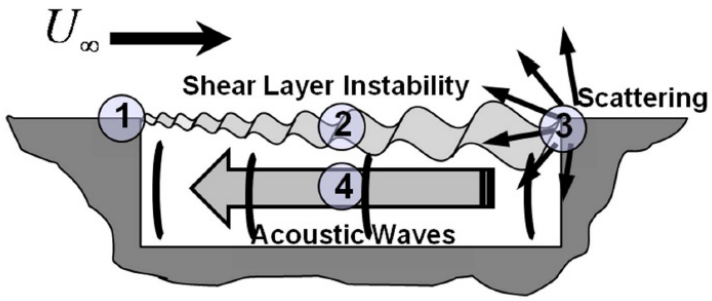

Figure 1. Schematic of cavity resonance generation mechanism.

Many studies have been conducted to predict the frequency at which these tones occur. Some of the earliest work was done by East [7] and Powell [8]. East's predictions were based on the normal modes of cavity resonance and were restricted to deep cavities at very low Mach numbers. At higher Mach numbers there were multiple tones in the cavity spectrum which were the harmonics of the primary tone. Powell used the edge tone phenomenon to explain the mechanism of self sustained acoustic resonance within the framework of the acoustic feedback loop. Rossiter [9] was the first to apply this model to cavity tones. The cavity tone resonance frequency is predicted using the equation,

$$St = \frac{fL}{u_\infty} = \frac{k-\beta}{M-1/\kappa} \tag{1}$$

Here, the coefficient κ is the ratio of the velocity of the convective disturbance (u_c) and free stream velocity (u_∞) and β in the phase lag between the passage of a hydrodynamic disturbance downstream past the cavity trailing edge and the formation of a corresponding upstream traveling acoustic disturbance. The values of both κ and β are chosen to best fit the experimental data. Rossiter suggested the values of κ and β to be 1/1.75 and 0.25 respectively. Later experiments by Heller, Holmes, and Covert [10] on shallow cavities showed that the resonant frequency for cavity flows could be better predicted using a slightly modified form of Rossiter's semi-empirical formula as given in following equation,

$$St = \frac{fL}{u_\infty} = \frac{k-\beta}{M\left[1+\left(\frac{\gamma-1}{2}\right)M^2\right]^{-1/2}+1/\kappa} \tag{2}$$

Using these relations one can easily predict the frequencies at which the cavity tones occur for various flow conditions. There have been numerous attempts to suppress cavity tones using a wide variety of flow control techniques, both passive and active in nature. The reviews by Cattafesta [11] and Rowley and Williams [12] provide the classification and methodology of cavity resonance control techniques. Some of the simplest methods are to add a spoiler at the leading edge of the cavity. The addition of the spoiler physically lofts the shear layer thereby reducing the interaction between the shear layer and the downstream edge of cavity. The other notable addition to the actuator list is the rod in cross flow. Early

investigations on this was conducted by McGrath and Shaw [13]. Stanek et al. ([14], [15], [16]) did extensive work on cavity tone suppression using a cylinder in cross flow. Bastrzyk and Raman [17] explored the use of rod on the ground to suppress the cavity flows. Further, the cavity resonance mechanism was studied using linear stability analysis by Panickar and Raman ([18]) and Sarpotdar et. al. ([19]). One other significant flow control actuator is the powered resonance tube actuator developed and described by Raman et. al. [20]. A detailed review of the evolution of the powered resonance tube actuator is given by Raman and Srinivasan [21]. Controlled unsteady mass addition was also used effectively as a flow control actuator. Raman [22] used unsteady mass injection to enhance jet mixing. Raman and Cain [23] compared the various innovative flow control actuators and Cain et. al. [24] simulated the powered resonance tube excitation of a boundary layer. Apart from these there are numerous other actuators that were tested to suppress cavity tones. These are listed in the review by Rowley and Williams [12].

1.2 Shock Tubes

A shock wave is a compression wave that moves through a fluid at a velocity greater than the velocity of sound in the undisturbed gas, producing an essentially discontinuous change from one thermodynamic state to another. The physical behavior of shock waves has been studied extensively since the mid-nineteenth century. One of the most common, simplest and earliest methods of generating these shock waves in a controlled laboratory environment is using shock tubes. The shock tube consists of a high pressure and a low pressure region separated by a diaphragm. The high pressure region is known as the compression chamber or driver tube and the low pressure region is known as the expansion chamber or the driven tube. When the pressure reaches the value of the rupture pressure of the diaphragm, the diaphragm is suddenly ruptured. Due to this event, the compression waves that coalesces into a normal shock wave propagates down the driven section while an expansion fan or rarefaction wave is pushed into the driver section. This shock wave causes a mass motion and forces the pressure in the driven section to rise along with the temperature, and the expansion wave decreases the pressure and temperature in the driver section. The point at which the driver and the driven gases meet and begin mixing is referred to as the contact surface or contact discontinuity. The contact surface, the region between the expansion fan and the normal shock moves at the same velocity and is the mass motion induced by the normal shock wave. Figure 2 shows the schematic of the mechanism of shock wave production in a shock tube. Depending upon whether the ends of the shock tube are closed or open, two different scenarios can occur. This phenomenon is represented in figure 3 using a wave diagram or a x-T diagram for a closed end shock tube. The X-axis is the position and the Y-axis is time.

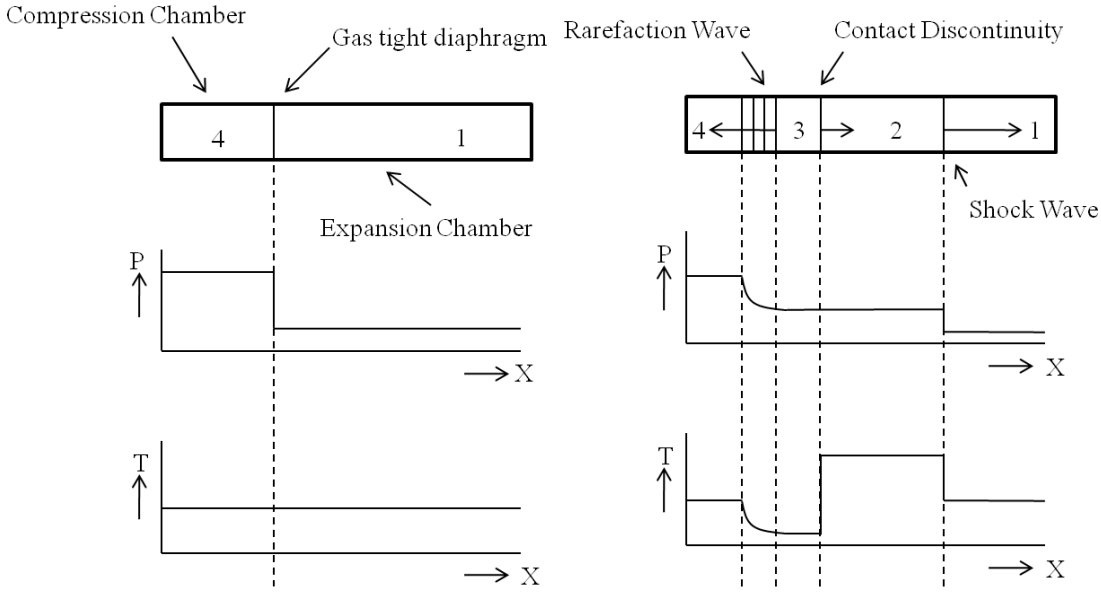

Figure 2. Schematic of shock wave generation mechanism along with the time and pressure history.

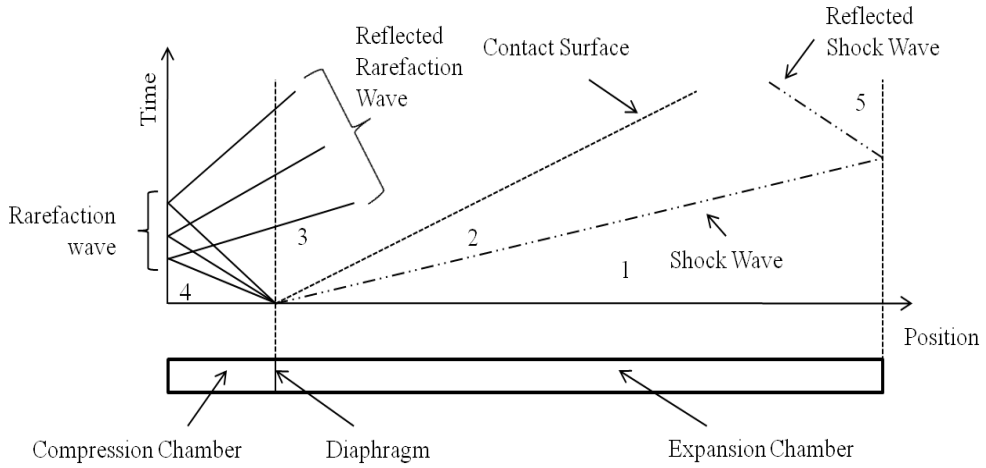

Figure 3. Schematic of shock tube mechanism with closed end shock tube illustrated with the help of a wave diagram.

When the diaphragm ruptures, a shock wave propagates in the expansion chamber and reaches the end of the shock tube the fastest and hence a line with low slope. The contact surface follows the shock wave and reaches the end of the shock tube after the shock wave has passed and so it is represented by a line with higher slope. Since the end is closed, the shock wave traveling in the expansion chamber interacts with the wall and gets reflected back as a shock wave. This reflected shock wave will interact with the contact discontinuity and produce multiple shock reflections. If the end of the compression chamber is open the expansion fan propagating into that chamber will be reflected back as an expansion wave. This mechanism is also illustrated in figure 3. Now if the ends of the shock tube are open then the shock wave traveling in the expansion chamber is reflected back as a expansion fan. The expansion waves that travel upstream of the shock tube gets reflected by the contact discontinuity as a reflected expansion wave. This reflected expansion wave will again be reflected from the open end, setting up a complicated interaction pattern. In the compression chamber, the propagating expansion fan is reflected back as a compression wave. This mechanism is shown in figure 4.

The characteristic equations which describe the events inside a shock tube can be easily derived using 1D shock wave theory. By using the equations of continuity, momentum, and energy the characteristic equation governing the shock tube flow is calculated to be,

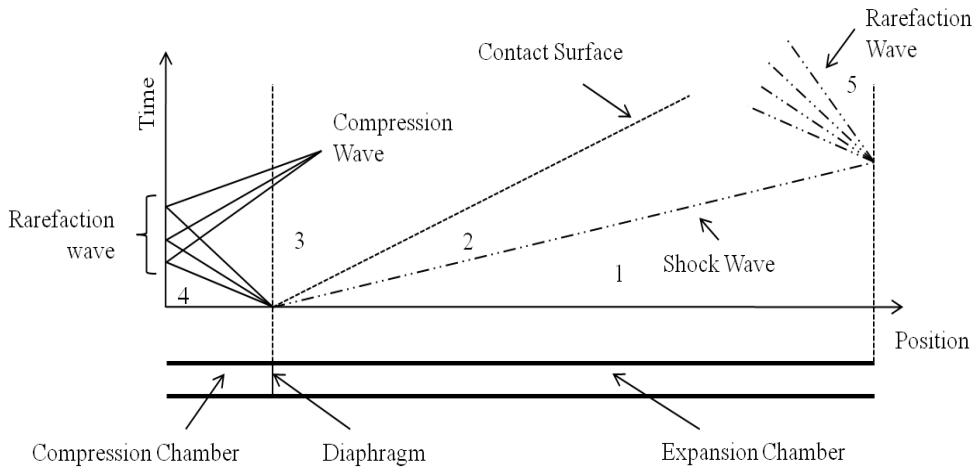

Figure 4. Schematic of shock tube mechanism with open end shock tube illustrated with the help of a wave diagram.

$$\frac{P_4}{P_1} = \frac{2\gamma_1 M_S^2 - (\gamma_1 - 1)}{\gamma_1 + 1}\left[1 - \frac{\gamma_4 - 1}{\gamma_1 + 1}\frac{a_1}{a_4}\left(M_S - \frac{1}{M_S}\right)\right]^{\frac{-2\gamma_4}{\gamma_4 - 1}} \quad (3)$$

Equation (3) relates the Mach number of the shock wave to the initial diaphragm pressure ratio. There are a few interesting things to be noted in this equation. Firstly, we observe that the Mach number of the shock wave is a function of two primary parameters; (a) the pressure ratio between the driver section and the driven section (P_4/P_1), and (b) the speed of sound ratio between the driver and the driven section (a_4/a_1). The speed of sound is determined by the specific heats, molecular weights and the temperature of the gases used in the driver and the driven section. This shows us that the strength of the shock wave can be controlled by changing either one or all of the following parameters; pressure of driver and driven section, type of gas used in driver and driven section, and the temperature of gases in the driver and driven section.

Since the advent of diaphragm shock tube by Vieille in 1899, the shock tube has been used in a variety of research studies such as chemistry, kinetics, wind tunnel studies and dynamics of hypersonic flight. The modern theory of shock tubes is treated in detail in books such as Courant and Friedrichs [25] and Rudinger [26], and the use of shock tubes is described in Wright [27] and Bradley [28]. Shock tubes were initially used to study the properties of gases at high temperatures and also to study aerodynamics at ever increasing velocities. Most of the chemical investigations were concerned with the actual reaction mechanisms behind the shock waves. The rapid increase in the use of the shock tube is due to its general simplicity, versatility and relative cheapness. Most of the shock tube research that has been conducted in the past are for relatively large shock tubes with diameters of the tubes greater than 0.5 m. Only recently, the problem of micro-scale shocks has received some attention, more specifically in the examination of the decaying properties of shocks in narrow channels [29] and the blast field surrounding microscopic explosive charges [30]. In parallel, materials scientists have been using localized high-energy deposition to study the properties of materials under extreme conditions [31] and also in non invasive drug delivery [32].

In order to use the shock tubes for experiments we need miniature shock tubes with diameters less than a centimeter. The real challenge is to develop miniature shock tube that can effectively produce shock waves that we can use using relatively cheap materials. We will look at the design and construction of such miniature shock tube in the following section.

2. DESIGN OF SHOCK TUBES AND EXPERIMENTS

The experiments conducted on the shock tube actuator were carried out in the high speed jet facility and anechoic chamber of the Fluid Dynamics Research Center (FDRC) at Illinois Institute of Technology. The anechoic chamber facility was used to conduct the characterization experiments whereas the testing of the shock tube as a flow control actuator was carried out in the high speed jet facility. The air supply to both these facilities was supplied from the compressed air supply system located in the basement of the E1 building at Illinois Institute of Technology. This section provides a brief description of the specifications and details of the shock tube design, experimental setup of various experiments, instrumentation used and finally data acquisition and post-processing techniques employed in this research.

2.1 Design of Shock Tubes and fast acting valve

In this section we discuss the different design considerations that went in to develop the various models of shock tubes used in this study. Two models of the shock tube, namely, single driver and multiple driver shock tube and one fast acting valve that produces steady or pulsed air injection are used in this study.

The most simple form of the shock tube is to have two rigid cylinder sections separated by a diaphragm. The single driver diaphragm type shock tube that was tested and used in this study is completely designed and built in-house. Figure 5 shows the various components of the shock tube. The shock tube consists of three main components; a driven section, a driver section and a diaphragm, essential for it to function. The driven section is made up of a 304 stainless steel tube of inner diameter 6.07 mm (0.239 in.) and outer diameter 6.35 mm (0.25 in.) and of length 76.2 mm (3.0 in.). One end of this tube is housed in a circular flange disc provided with holes to accommodate allen screws. Together the tube and the flange make up the driven section. The driver section is also made up of the same stainless steel tube but of length 25.4 mm (1.0 in.). The entire tube is housed in a circular flange disc

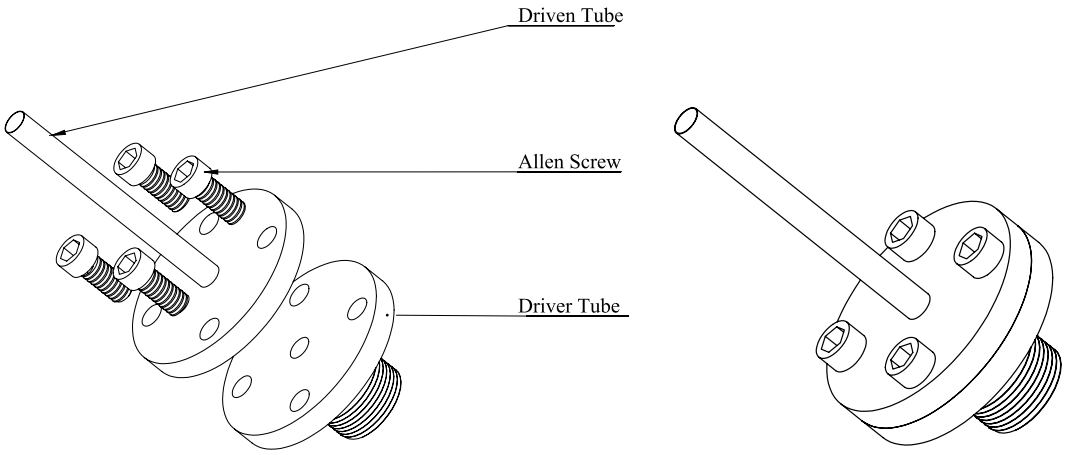

Figure 5. Schematic of the single driver shock tube.

which is provided with threaded holes to accommodate allen screws and the shaft of the flange disc is threaded so that it can be fitted to the compressed air facility. Together, the tube and flange housing make up the driver section. For the diaphragm, two different materials were tested, namely, a soft tempered aluminum foil of thickness 0.0127 mm (0.0005 in.) and a clear mylar sheet of the same thickness. The diaphragm material is placed between the driver and the driven sections along with an O-ring to ensure an air tight seal between the two sections. The two sections are fastened using allen screws. During preliminary testing it was observed that providing a chamfer of 45^0 at the flange end of the driven tube helped in clean rupture of the diaphragm. This feature is incorporated in all the diaphragm type shock tubes. In order to study the characteristics of the shock tube, a shock tube which could house the pressure transducers was required. Figure 6 shows the schematic of the instrumented single driver diaphragm type shock tube. The tubes used for the driver and driven section are the same as mentioned before. The design of the driven section is similar to the one described above whereas the driven tube was designed to house the pressure transducers. The length of the driven tube is 152.4 mm (6 in.) in this case and is housed in a hollow shaft with a flange disc at one end and with a cap on the another end. The shaft is milled on opposite sides to have flat surfaces as shown in figure 6(a). Five holes are drilled on each of these surfaces one inch apart from each other so as to accommodate the pressure transducers. At the end of the shock tube a cap is provided which is used to close the end of the shock tube. The cap is fastened to the end of the shaft using allen screws. The shock tube is assembled using the same procedure as above and a schematic of the assembled instrumented shock tube is shown in figure 6(b).

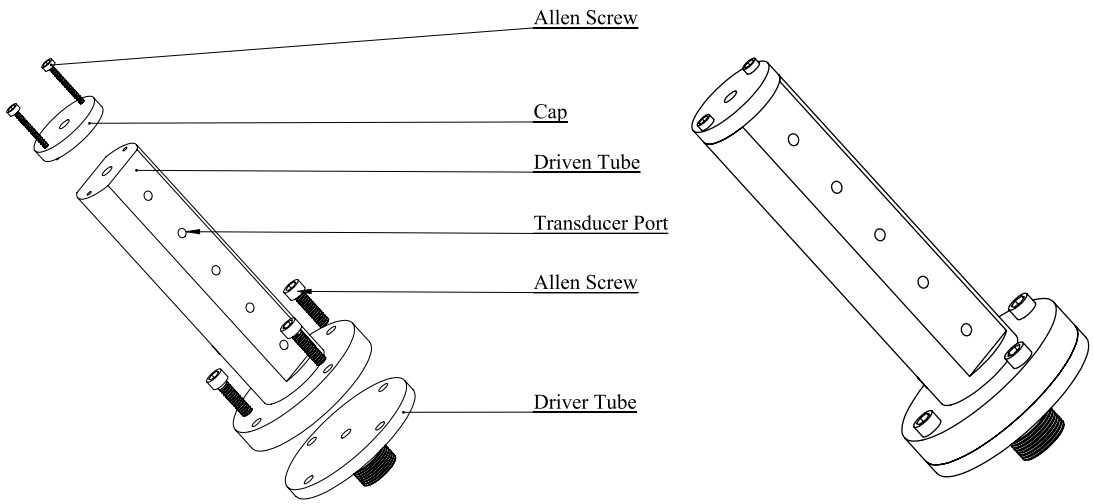

Figure 6. Schematic of the instrumented single driver shock tube.

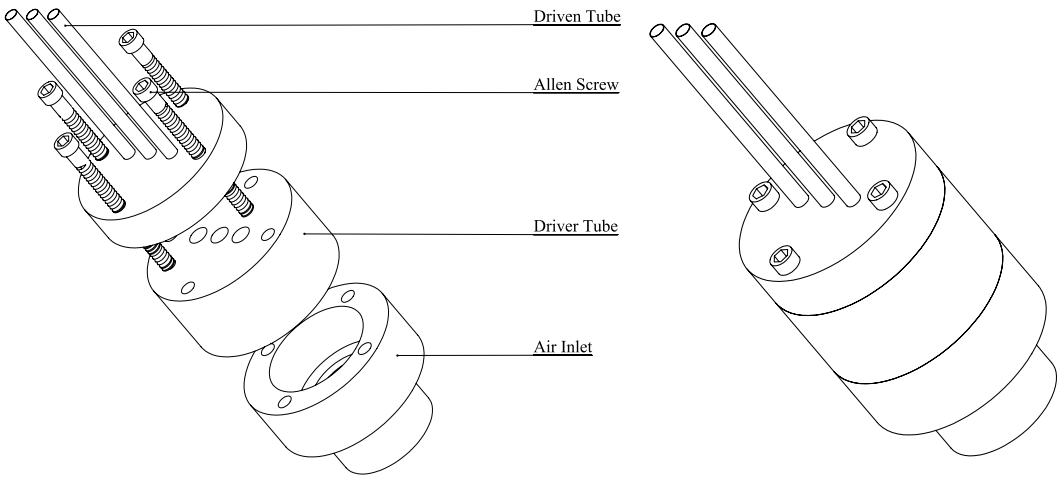

Figure 7. Schematic of the multiple driver shock tube.

The concept of a multiple driver diaphragm type shock tube serves to maintain the same exit cross sectional area as the single driver shock tube but to divide the total area into three smaller diameter shock tubes and distribute them evenly along the span of the cavity. This actuator was also designed and constructed in-house. Similar to the design of the single driver shock tube, we have a driven section and a driver section separated by a diaphragm. The driver section consists of three 304 stainless steel tubes of inner diameter 3.81 mm (0.15 in.), outer diameter of 4.06 mm (0.16 in.) and a length of 76.2 mm (3.0 in.). The three tubes were fitted on to a flange disc with the bottom edge chamfered to 45^0. The driver section consisted of three 304 stainless steel tubes of inner diameter of inner diameter 6.07 mm (0.239 in.), outer diameter 6.35 mm (0.25 in.) and of length 25.4 mm (1.0 in.). The three tubes were housed in a circular block as shown in figure 7(a). The driven section is fitted with the driver section with a diaphragm and an O-ring between them. The driver section is fitted on top of an air supply block which is a circular block that is attached to the compressed air supply line. The schematic of fully assembled multiple driver shock tube is shown in figure 7(b).

In order to produce steady and pulsed mass injection, a 2/2-way, closed, single solenoid valve is employed. These valves can be operated by a 24 V DC supply with a 3 - 30 VDC trigger signal. The working pressure range for this valve is 0.05 MPa (7.25 psig) to 0.6 MPa (87 psig) with a standard nominal flow rate of 100 liters per minute. The maximum switching frequency for this valve is 1000 Hz. The response time of the solenoid valve is 0.8 - 0.9 ms for switching on and 0.4-0.5 ms for switching off. A schematic of the valve is shown in figure 8. The inlet to the valve is connected using a flexible polyurethane tube of inner diameter 3.81 mm (0.15 in.), outer diameter 6.35 mm (0.25 in.) and a length of 25.4 mm (1.0

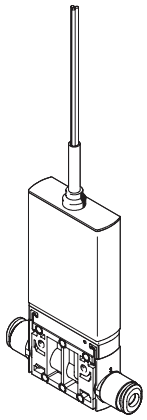

Figure 8. Schematic of the fast acting solenoid valve.

in.). The outlet of the valve is also connected to the same type of tube but with a length of 76.2 mm (3 in.). The maximum pressure that the tube can hold is 1.03 MPa (150 psig) at ambient conditions.

2.2 Cavity apparatus and high speed flow facility

The setup used for the cavity flow experiments was designed in-house. Figure 9 shows the schematic of the cavity flow experimental setup. The setup consists of three components, namely, cavity block, shock tube adapter and a baseplate. The cavity block is an aluminum block with a rectangular slot of dimensions 25.4 mm x 50.8 mm x 12.7 mm (2.0 in. x 1.0 in. x 0.5 in.) cut out from it. Holes are drilled on the shock tube adapter to accommodate the driven section of different models of shock tubes used during this research. The shock tube adapter is an aluminum block of dimensions 19.0 mm x 25.4 mm x 12.7 mm (0.75 in. x 1.0 in. x 0.5 in.). All these components are separately shown in Figure 9(a). The adapter and the cavity block are mounted on the baseplate as shown in Figure 9(b). This results in a cavity (L/D=2) with dimensions of length L = 25.4 mm, width W = 25.4 mm, and depth D = 12.7 mm (1.0 in. x 1.0 in. x 0.5 in.). This cavity flow setup is mounted flush with the bottom edge of the rectangular nozzle of dimensions 10.17 mm x 50.80 mm. (0.4 in. x 2.0 in.) cut out on a circular flange disc attached to the high speed jet facility. The jet flow over this block provides the freestream air that flows over the cavity. The jet exhausts into a ducted anechoic chamber. The baseplate and the shock tube adapter of the cavity block were modified to accommodate the various shock tubes and fast acting valves. The cavity along with the multiple driver shock tube was mounted on to the jet facility with a spacer block between them. The schematic of the complete assembly is shown in figure 10.

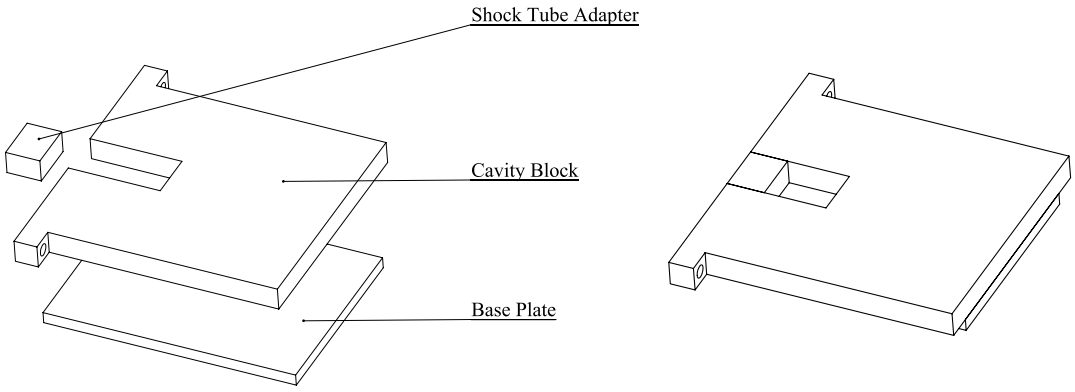

Figure 9. Schematic of the cavity block used for cavity flow control experiments.

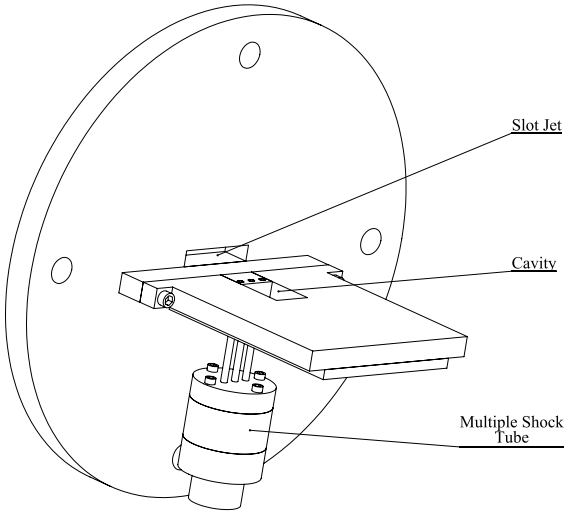

Figure 10. Schematic of the cavity flow control experimental setup with the multiple driver shock tube mounted upstream of the cavity. The cavity block with the shock tube is mounted on the rectangular slot jet of the high speed jet facility.

2.3 Data acquisition and Instrumentation

The acoustic measurements were made using a 6.25 mm (0.25 in.) diameter Bruel & Kjaer microphone (Type 4939). All microphones were calibrated before each run using a Bruel & Kjaer pistonphone (Type 4228). For the dynamic pressure measurements Kulite pressure transducers (Types XCS-062, XTEL-190-250A and XTL-140-100A) were used. For the velocity measurements, a hypodermic pitot probe attached to a Kulite (XCS-062-25D) transducer was used. The pitot probe had an internal diameter of 0.1016 mm (0.004 in.) and external diameter of 0.2032 mm (0.008 in.). The mean value of the signal measured by the pitot probe at a point was used to calculate the stagnation pressure and subsequently, the axial velocity, at that point. The stagnation pressure monitoring in the compressed air facilities and jet facility was done using a Setra pressure transducer. The signal from each transducer was bandpass filtered using an Ithaco analog filter (Model 4212). The filter settings varied depending on the experiment and these setting will be discussed with the experimental methodology. The analog data acquired from the sensors and transducers was digitized using a National Instruments data acquisition card, the PCI-MIO-16E-1. This is a 12-bit multifunction data acquisition card with a maximum sampling rate of 1.25 MS/s and up to 16 analog inputs. For high speed sampling a different data acquisition card was used (NI-PCI-6133). This is a 14-bit card with a maximum sampling rate of 2.5 MS/s. The DAQ cards were connected to a connector board interface BNC-2110. Apart from this a NI USB-6211 DAQ card was used to transfer the control signal to the solenoid valve. This is a 16-bit card with a maximum sampling rate of 250 kS/s. For the phase averaged measurements, the measurement signal was obtained from a Kulite pressure transducer at several points on a prefixed measurement plane. Once both the reference and measurement signals were acquired simultaneously using appropriate filter settings to avoid aliasing, the reference signal was bandpassed filtered around the frequency of interest. This left us with, ideally a pure sinusoidal wave. The time period of the signal was determined based on the time difference between two consecutive peaks. Then, each of these time periods was divided into a suitable number of phase angles (in our case, 24 angles) and corresponding time for these different phases recorded. Now for the corresponding times pressure information from the measurement signal was sought. This information was then averaged out for a particular phase. The graphical programming language LabVIEW was used for the actual data acquisition, generating control signal, pre processing and data storage. The post processing and plotting of the acquired data was done using Matlab 8.0. The designing of shock tubes was done using SolidWorks.

3. RESULTS AND DISCUSSION

The results of the experiments are discussed in two parts. The characterization experiments were performed on the shock tubes and the fast acting solenoid valves to understand the behavior of these actuators. Once the behavior of the actuators was understood they were used in cavity flow control experiments to evaluate their efficacy in suppressing the cavity noise. The results of these experiments are discussed in detail below.

3.1 Characterization of Shock Tubes

One of the important aspect of the diaphragm type shock tube is the type of diaphragm used. There are many suggested diaphragm materials in the literature, among them are cellulose acetate, aluminum foil, mylar, and a few others. In our case we needed diaphragms of very small thickness considering the area exposed to the flow was small in case of miniature shock tubes. Two diaphragm materials which were commercially available at very small thickness were aluminum foil and mylar sheet. Three tests were conducted to select a suitable diaphragm which not only produced shock waves but also produced reproducible data. Experiments were conducted using the single driver diaphragm type shock tube by using all the three diaphragm to see if they produced shock waves. Figure 11(a) shows the pressure time history of a pressure transducer located at the exit plane of the single driver shock tube facing the flow. In this case the diaphragm used was a single aluminum foil of thickness 0.0127 mm (0.0005 in.). From the figure we observe that the structure of the shock wave corresponds to that expected based on 1-D theory. Initially, after the diaphragm burst we observe a shock wave that travels down the expansion chamber (Region 1-2). Behind the propagating shock wave is a contact discontinuity across which the pressure has to remain constant (Region 2-3) and the flow through the expansion fan propagates into the compression chamber which travels down the tube (Region 3-4). Finally, the mass flow from the compressor exits the shock tube. This structure is clearly visible from the pressure time history at the

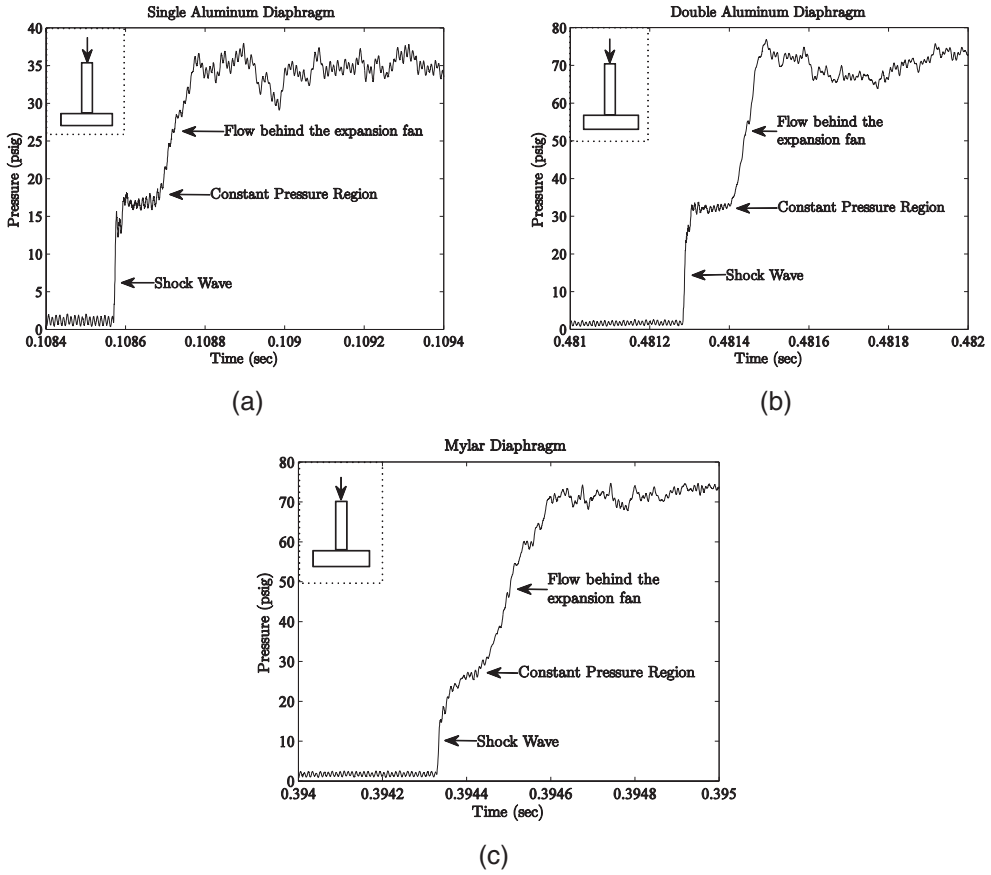

Figure 11. Pressure time history of the single driver shock tube with, (a) single aluminum foil, (b) double aluminum foil and (c) mylar as the diaphragm. The arrow in the figure indicates the location of the pressure transducer.

exit of the shock tube. The initial diaphragm pressure ratio (P_4/P_1) was maintained at 5.42 and both the driver and driven gases are air at atmospheric temperature. Figure 11(b) shows the pressure time history of a pressure transducer located at the exit plane of the single driver shock tube with two aluminum foils of thickness 0.0127 mm (0.0005 in.) as diaphragm. The initial diaphragm pressure ratio (P_4/P_1) was maintained at 7.12 and both the driver and driven gases are air at atmospheric temperature. We observe that in this case a stronger shock is produced when compared to the single aluminum diaphragm case. The structure of the shock wave once again correlates with the theory. One of the main drawbacks of using double aluminum diaphragm was the repeatability. The double aluminum diaphragm did not have good burst pressure repeatability. Strong fluctuations in burst pressure (about 10 to 15 psig) were observed. Figure 11(c) shows the pressure time history of a pressure transducer located at the exit plane of the single driver shock tube with mylar sheet of thickness 0.0127 mm (0.0005 in.) as diaphragm. The initial diaphragm pressure ratio (P_4/P_1) was maintained at 7.8 and both the driver and driven gases are air at atmospheric temperature. The strength of the shock wave seemed to be weak in the case of the mylar diaphragm. This could be attributed to the tensile nature of the mylar sheet. One could visually observe the mylar sheet bulge out before rupture in a tensile nature. In case of aluminum, once the rupture pressure is reached the aluminum shattered and did not undergo tensile deformation. Due to the fact that the single aluminum diaphragm shock tube had good repeatability, it was decided to use the single aluminum diaphragm as the primary diaphragm for the rest of the study.

In the theory of shock tube we came across the two different scenarios possible in a shock tube. One when the end of the shock tube is closed and another when it is open. Figure 12(a) shows the pressure time history of the pressure transducer located three inches from the diaphragm of a single driver instrumented shock tube. The pressure transducer was placed perpendicular to the axis on the wall of the shock tube to measure the static pressure. From the figure we observe the complex interaction

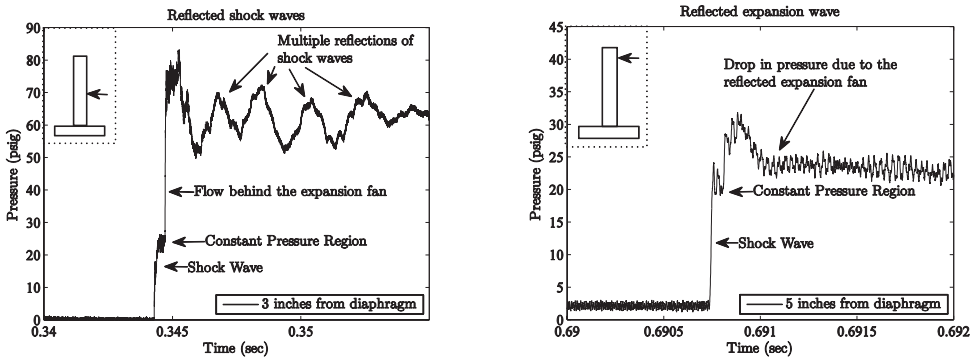

(a) (b)

Figure 12. Pressure time history of the single driver shock tube with a single aluminum foil as diaphragm and with the end (a) closed and (b) open. The arrow in the inset figure indicates the location of the pressure transducer.

pattern of multiple reflected shock waves. This correlates with theory which tells us that when the end of the shock tube is closed the shock waves get reflected back as shock waves and further interact with the flow and create a complex flow pattern with multiple shock waves and expansion waves. Figure 12(b) shows the pressure time history of the pressure transducer located five inches from the diaphragm of a single driver instrumented shock tube. The pressure transducer was placed perpendicular to the axis on the wall of the shock tube to measure the static pressure. We observe the initial structure of the shock wave following which there is a sudden drop in pressure. This is due to the reflected expansion fan from the open end. This correlates with theory which tells us that when the end of the shock tube is open the shock waves get reflected back as expansion waves which propagate back into the expansion chamber. There is one final check which needs to be done i.e., the comparison of theoretical and actual velocity of the shock wave. In order to calculate the actual velocity of the shock wave, two pressure transducers were placed perpendicular to the axis on the walls of the shock tube separated by a distance of two inches. By knowing the time difference (Δt) between the shock wave reaching the pressure transducer located at three inches from the diaphragm and the pressure transducer located at five inches from the

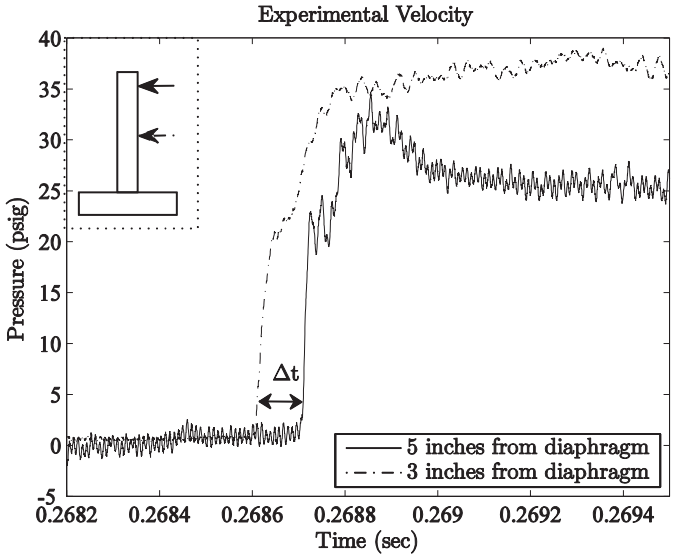

Figure 13. Static pressure time history of the single driver shock tube with a single aluminum foil as diaphragm at 3 and 5 inches from the diaphragm. The time delay is used to calculate the velocity of the wave.

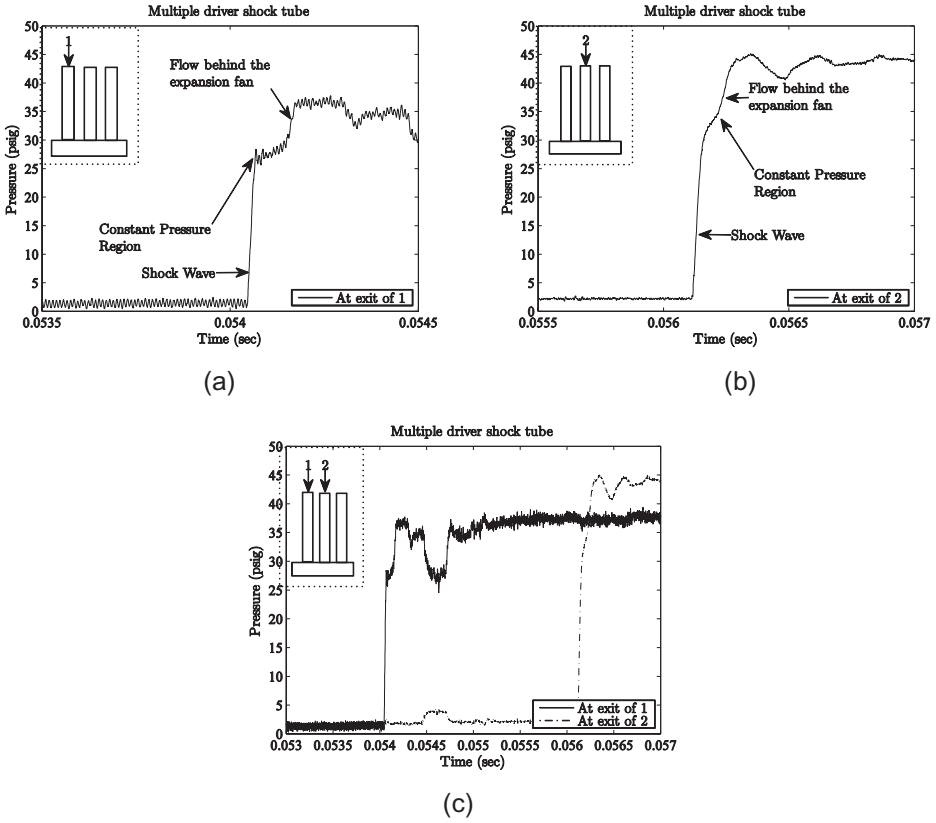

Figure 14. Total pressure time history of the multiple driver shock tube with single aluminum foil as diaphragm at the exit of,(a) the first shock tube, (b) the second shock tube and (c) both simultaneously.

diaphragm, we calculate the actual velocity. Figure 13 shows the pressure time history of both the pressure transducers located two inches apart. The actual velocity was calculated to be 502.4 m/s. The theoretical Mach number was calculated from the eqn (3) and using the speed of sound relation, the theoretical velocity was calculated to be 508 m/s. The error between theoretical and actual velocity was found to be less than 2 %. This shows that the miniature single driver shock tube produce shock waves comparable to that defined by theory.

The main idea behind using a multiple driver diaphragm type shock tube is to distribute the energy of the shock across the span of the cavity width rather than using a centrally located shock tube. Figure 14(a) shows the pressure time history of a pressure transducer located at the exit of one of three shock tubes (1) along the axis, facing the flow. We observe that the shock wave has a similar structure to the one we observed in single driver shock tube. The diaphragm material used here was a single sheet of aluminum foil of thickness 0.0127 mm (0.0005 in.) and the initial diaphragm ratio was maintained to be 5.76. The driver and the driven gases were air at standard atmospheric temperature. Figure 14(b) shows the pressure time history of a pressure transducer located at the exit of one of three shock tubes (2) along the axis, facing the flow. Here too we observe that the shock wave has a similar structure to the one we observed in single driver shock tube. Figure 14(c) shows the pressure time history of two pressure transducers located at the exit of two adjacent shock tubes of the multiple driver shock tube. We observe a small time delay between both the pressure signals indicating that the diaphragm does not burst at the same instant at all the three shock tubes. The experiment was repeated to determine the phase lag between the tubes and was observed that it was not constant and appeared to be random. This could be attributed to the fact that aluminum foil used may include some material deformities or non uniform material thickness throughout, due to which one of the shock tubes generates a shock wave a little later than the other.

The fast acting solenoid valves are used to study the effect of steady and pulsed blowing on the

cavity noise generation mechanism. The internal diameter of the tube fixed to the exit of the valves is same as the internal diameter of the multiple driver shock tubes. Figure 15(a) shows the pressure time history of the pressure transducer placed at the exit of the fast acting valve along the axis, facing the flow. A closer look at the pressure signal reveals that the valve does not produce any shocks at the exit of the valve. This indicates that the solenoid valve produces a steady stream of air at the exit (no shock waves). Figure 15(b) shows the pressure time history of signal from the pressure transducer located at the exit of the valve along the axis, facing the flow. The actuator in this case is pulsing air at a frequency of 5 Hz. The input signal to the valve was a square wave which is evident from the pressure signal. The structure of the pressure time series resembles a ON-OFF nature of the valve. During the OFF cycle there is no air coming out of the exit of the valve and hence the pressure transducer reads no pressure. Whereas during the ON cycle steady air is being injected out from the exit of the valve and hence the pressure transducer reads a mean pressure value of about 33 psig. The flow from these valves was supersonic with a Mach number of 1.42. Figures 15(c-f) shows the pressure time history of the pressure transducer located at the exit of the valve along the axis, facing the flow. The valves are pulsing at

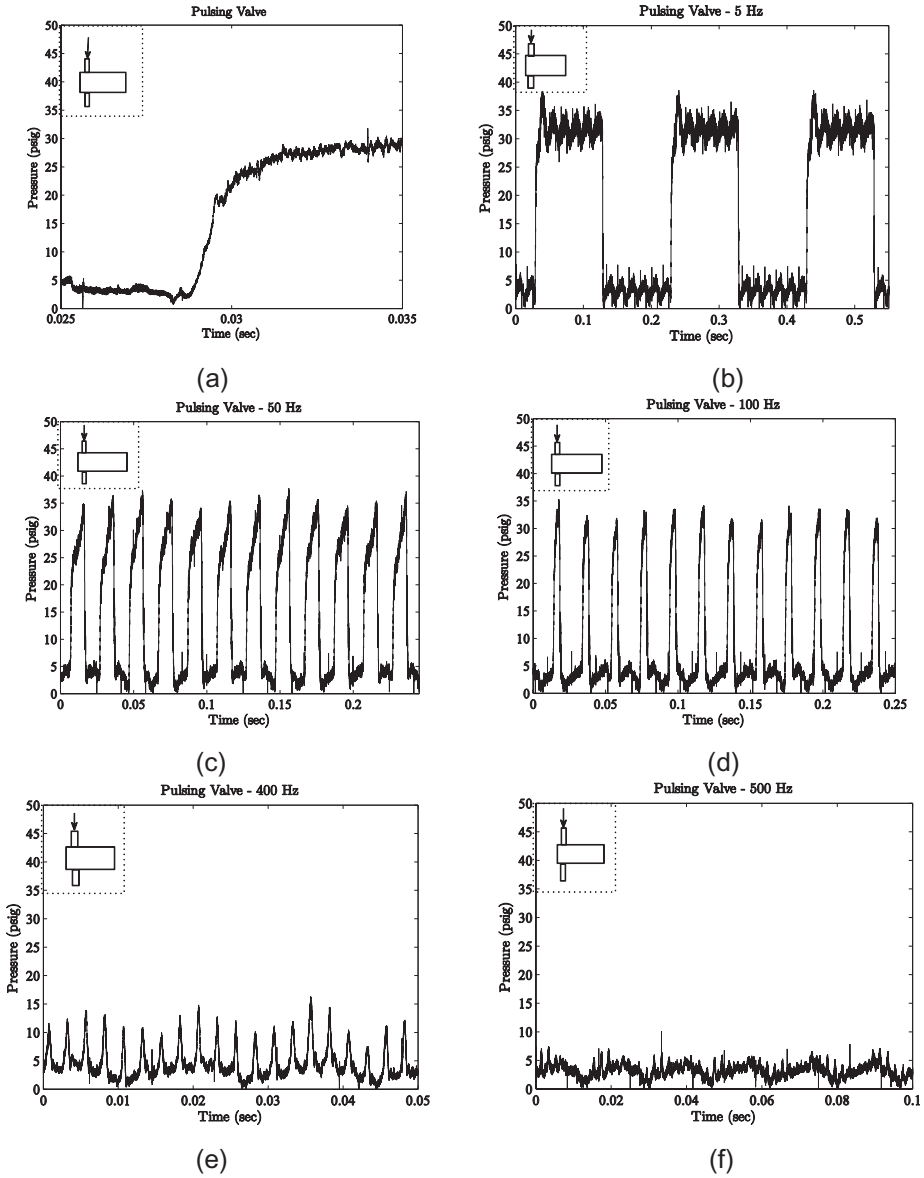

Figure 15. Pressure time history of the fast acting solenoid valve measuring the total pressure at the exit of valve pulsing, (a) once, (b) at 5 Hz, (c) at 50 Hz, (d) at 100 Hz, (e) at 400 Hz and (f) at 500 Hz.

frequencies of 50, 100, 400 and 500 Hz respectively. In these figures we observe that as we move towards higher frequencies the ON-OFF nature at the valve exit transforms into a peak to peak impulsive flow. It is also interesting to notice that the pressure at the exit gradually decreases as we move towards higher actuation frequencies. We observe from Figure 15(d) that at the actuation frequency of 500 Hz or higher the valve exit pressure diminishes to less than 10 psig.

3.2 Cavity flow control

In this section, we present experimental results depicting the effectiveness of the shock tube and fast acting solenoid valve actuators in reducing the tonal noise occurring due to the resonant cavity tone mechanism. A comparison will be made between the various methods i.e., the effect of shock and the effect of steady and pulsed mass injection. Acoustic measurements from a calibrated microphone will provide the actual noise suppression that resulted due to the two actuators. The velocity profile and phase averaged pressure measurements will help in determining the mechanism by which these actuators suppress the cavity tone.

Before we look at the effect of the actuators on the cavity tone, we examine the baseline spectrum of the cavity. Here we refer to baseline case as the condition where there is no actuator is used. We refer to the case when the actuators are used as the controlled case. Figure 16 shows the SPL - frequency spectrum of three baseline cases at three different Mach numbers, namely, M = 0.6, 0.7 and 0.8. The frequency at which the tonal noise occurs could be predicted by the Rossiter tone equation given by eqn (1). From the figure we observe that the SPLs of the three cases were more or less constant at about 125 dB. The frequencies at which the tone occurs however changes with Mach number. The tonal noise for M = 0.6 flow occurs at $f_{0.6}$ = 3204 Hz, for M = 0.7 the flow occurs at $f_{0.7}$ = 3357 Hz and finally for M = 0.8 at $f_{0.8}$ = 3586 Hz. On comparing these results with the Rossiter formula, we observed that the second Rossiter mode is the dominant one for this particular cavity.

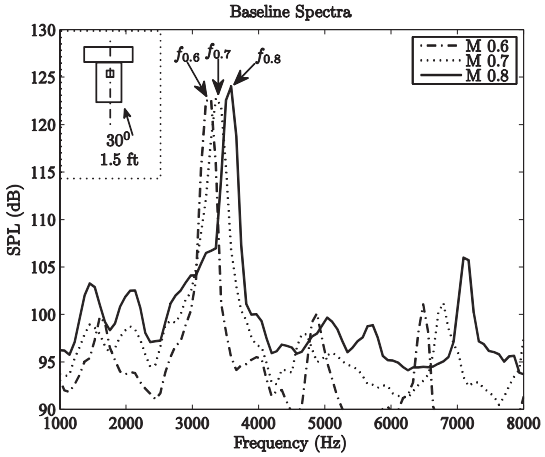

Figure 16. Sound pressure level (SPL)- frequency spectra for flow over a cavity at Mach number 0.6, 0.7, and 0.8. The microphone was positioned at 30^0 to the jet axis and at a distance of 0.45m (1.5ft) from the jet axis.

Now let us investigate the effect of the shock in reducing cavity tone noise. The shock tube used in this case was a single driver shock tube with a single aluminum foil as diaphragm. Figure 17(a) shows the pressure time series of the single driver shock tube with a M = 0.6 flow over the cavity. The shock tube is actuated around 0.3 s. Before this time the flow over the cavity is considered to be the baseline case. Once the diaphragm ruptures and the shock wave exits through the shock tube, we observe a sudden drop in pressure followed by an increase in pressure. Upon repeating the experiment several times we still observe the same behavior when the shock tube is actuated. This gives us reason to believe that this "convergent-divergent effect" in the time series is due to the presence of the shock wave exiting the shock tube. Figure 17(b) shows the SPL - frequency spectrum of the single driver shock tube with M = 0.6 flow over the cavity. In this case we observe the cavity tone suppression due to the shock to be about 6.5 dB (this suppression was for the time interval 0.285 s to 0.3 s). The

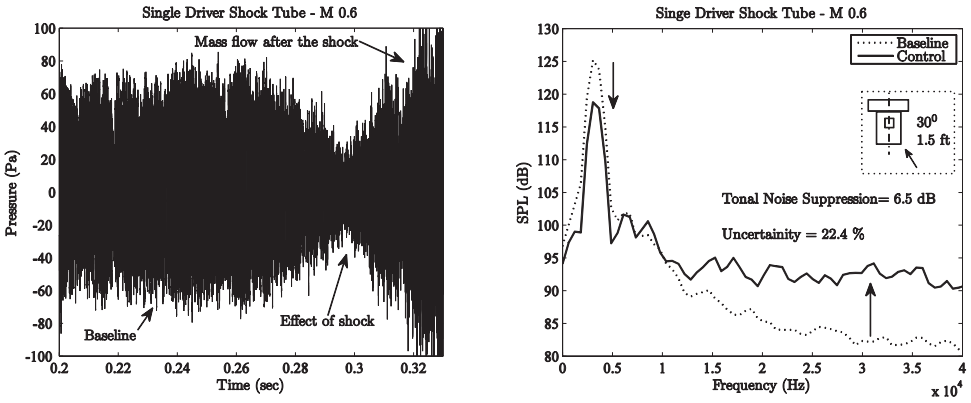

(a) (b)

Figure 17. Pressure time history and SPL frequency spectrum showing the effect of single driver shock tube on the noise generated by a M 0.6 flow over the cavity.

uncertainty in this case is about 22.4%. The broadband noise begins to increase around 12 kHz and increases by almost 10 dB for frequencies greater than 20 kHz during this time. Figure 18(a) shows the pressure time history of the single driver shock tube with a M = 0.8 flow over the cavity. Here too we observe the decrease in pressure due to the shock as observed in the M = 0.6 case. However the decrease in the pressure is less when compared to the M = 0.6 case. The shock tube was actuated at around 0.09 sec. Figure 18(b) shows the SPL- frequency spectrum for the same case. We observe that the reduction on the cavity tone amplitude in this case is only about 2.4 dB as compared to 6.5 dB in the M = 0.6 case. Similar to the M = 0.6 case we also observe increase in the broadband noise for frequencies greater than 20 kHz.

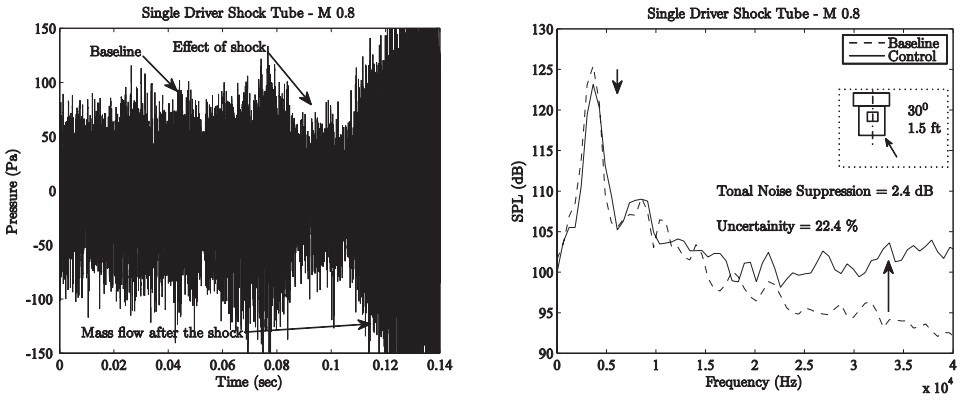

(a) (b)

Figure 18. Pressure time history and SPL frequency spectrum showing the effect of single driver shock tube on the noise generated by a M 0.8 flow over the cavity.

As we observed in the single driver shock tube case, the shock wave has a significant effect on suppressing the cavity tone noise. The main idea behind the multiple driver shock tube is to maintain the same exit area as the single driver shock tube but divide the shock tube into three smaller shock tubes and distribute them across the span of the cavity width. We believe that this spatial distribution of the shock tube will result in higher suppression of the tonal noise. Figure 19(a) shows the pressure time history of the multiple driver shock tube with M = 0.6 flow over the cavity. In this case, again we clearly observe the effect of the shock. The pressure drop in this case is significant and persists for a longer period of time. Figure 19(b) shows the SPL - frequency spectrum of the same case. We observe

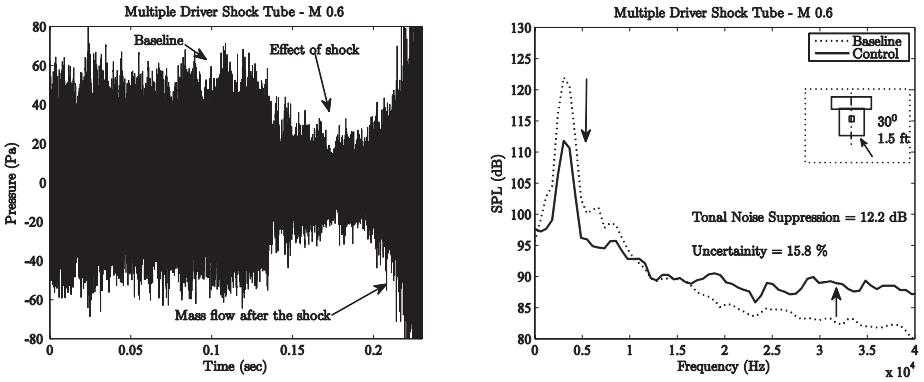

(a) (b)

Figure 19. Pressure time history and SPL frequency spectrum showing the effect of multiple driver shock tube on the noise generated by a M 0.6 flow over the cavity.

a 12.2 dB suppression of the cavity tonal noise. It is also interesting to observe the increase in the broadband noise has reduced to about 5 dB. The uncertainty of measurement in this case was 15.8%. This shows the effectiveness of dividing the shock tubes and spreading them through the span of the cavity width. Figure 20(a) shows the pressure time history of the multiple driver shock tube with M = 0.8 flow over the cavity. When compared to the M = 0.6 case, here we observe that the shock tube still has significant effect on the cavity tone. The effect of the shock is clearly visible in the pressure time history. Figure 20(b) shows the SPL - frequency spectrum. The tonal noise is suppressed by about 10 dB with an uncertainty of 17.4%. A slight increase in the broadband noise for frequencies greater than 20 kHz is also observed. This shows the effectiveness of the multiple driver shock tube at high subsonic Mach numbers. One interesting observation made in both the types of shock tube actuators was that the shock which was about 0.3 ms in duration had a suppressing effect on the cavity tone for about 20 ms. This kind of 'memory effect' is commonly observed in resonant acoustics. The potential drawback of the shock tube actuators in its current form is the inability to produce periodic shock waves in quick succession. This effort was designed to document the effectiveness of the shock waves in suppressing cavity noise.

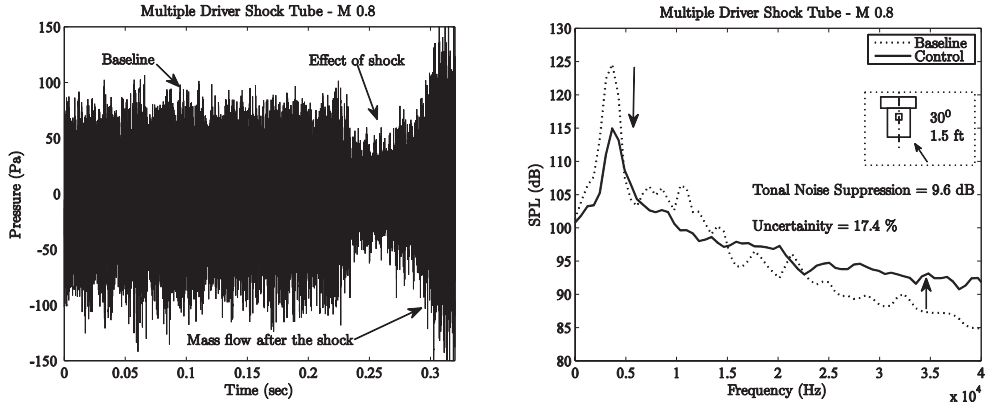

(a) (b)

Figure 20. Pressure time history and SPL frequency spectrum showing the effect of multiple driver shock tube on the noise generated by a M 0.8 flow over the cavity.

It was of interest to see how the effect of a shock wave on cavity tone was different from that of steady or pulsed mass injection. Figure 21 (a) shows the pressure time history of the microphone that shows the effect for steady mass injection of duration 1 s injected into the system. We observe that there

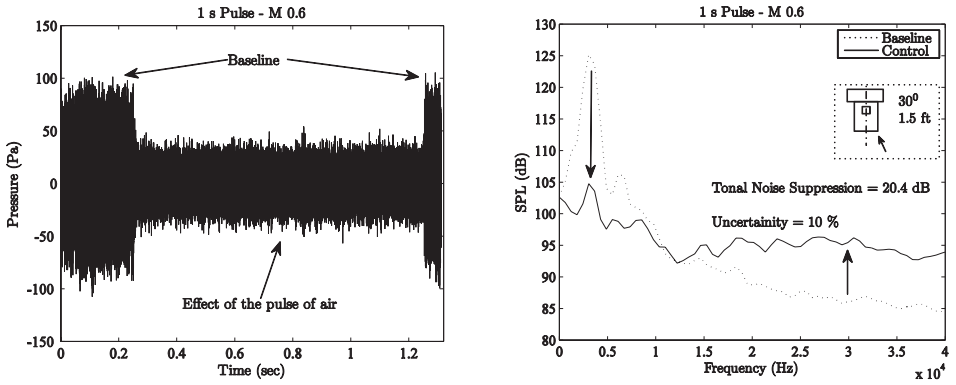

(a) (b)

Figure 21. Pressure time history and SPL frequency spectrum showing the effect of 1s pulse of air from the fast acting solenoid valve on the noise generated by a M 0.6 flow over the cavity.

is a significant drop in pressure during this time. Upon close investigation we observe that the pressure drop observed is exactly for the duration of the pulse of air i.e., 1s. After, this the cavity tone immediately reappears once the mass injection is stopped. The 'memory effect' observed in the shock tube case was absent in this case. This shows that the behavior was unique to the shock tube case. Figure 21(b) shows the SPL - frequency spectrum of the 1s air injection case. The baseline case has a tonal amplitude of about 125 dB. Due to the 1s pulse of air the cavity tone is suppressed up to 20 dB. Figure 22 shows the pressure time series and the SPL - frequency spectrum of the fact acting valve pulsing at 5 Hz. The actuator is fed with a ON-OFF type square signal of frequency 5 Hz. From the time series we observe the continuous suppression and occurrence of the cavity tone. As observed in the previous results, here too the suppression occurs only for the duration of the ON cycle of the valve during which the tonal noise is suppressed by 19.2 dB. The broadband noise begins to increase slightly for frequencies greater than 12 kHz and increases by about 10 dB for frequencies greater than 20 kHz. Figure 23 shows the SPL - frequency spectrum of the fast acting valve pulsing at 100 and 500 Hz with M = 0.6 flow over the cavity. We observe that there is minimal suppression of the peak tonal noise (2-3 dB) occurring at the dominant Rossiter mode ($f_{0.6}$). We also observe that the harmonics of the Rossiter mode frequency are completely or partially suppressed in both the cases. In case of the valve actuation frequency of 500 Hz, we clearly observe the energy component (f_{500}) due to the valve pulsing in figure 23(b). The SPL magnitude that was introduced due to the pulsing of the valve is about 105 dB. The main reason for the failure of the pulsing valve in reducing the cavity tone is that at high pulsing

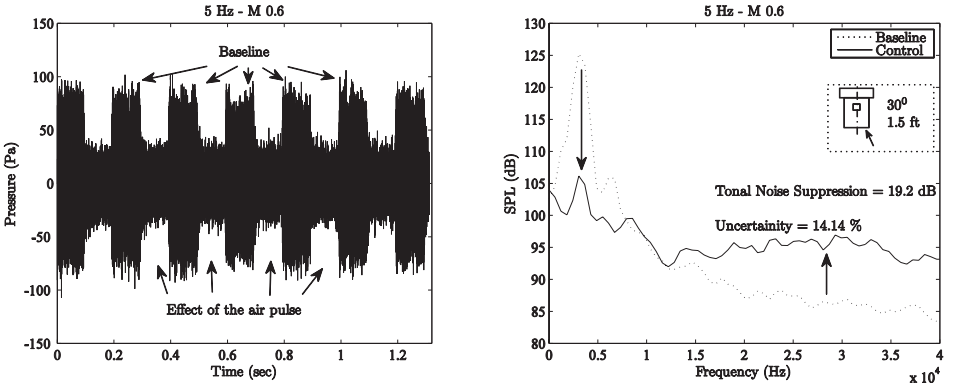

(a) (b)

Figure 22. Pressure time history and SPL frequency spectrum showing the effect of the solenoid valve pulsing at 5 Hz on the noise generated by a M 0.6 flow over the cavity.

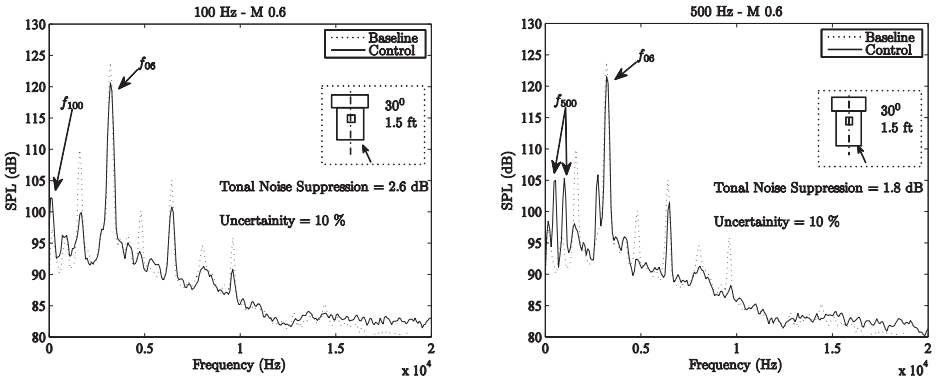

(a) (b)

Figure 23. SPL frequency spectrum showing the effect of the solenoid valve pulsing at (a) 100 Hz and (b) 500 Hz on the noise generated by a M 0.6 flow over the cavity.

frequencies the pressure at the exit of the valve diminishes to a mere 10 psig in case of 500 Hz as discussed in the previous section.

At this point a discussion on the mass flux and the momentum coefficient of these actuators is pertinent. The mass flow rates and momentum coefficients[3] (C_μ) of the three different actuators under study are shown in Table 1. The momentum coefficients for the shock tubes are calculated based on the memory effect discussed earlier by imposing a duty cycle. This is based on the assumption that the shock of duration 0.3 ms is sufficient to suppress the cavity tone for a duration of 20 ms. The mass flow rate of the actuators are expressed in terms of percentage of mass flow rate of the main jet. We observe that the mass flux and the momentum coefficients of the fast acting solenoid valve are very high for a flow control actuator. Whereas the values for the shock tube actuators are much lower based on the assumed duty cycle. The idea behind this is to develop a device which can generate shock waves periodically in quick succession. This type of shock tube actuator will have low mass flux and momentum coefficient, while at the same time having high control authority.

Table 1. Momentum coefficient of the actuators and total mass flow rate of the actuators as a percentage of main jet mass flow rate.

Actuator	Mach number of jet (M)	Mass flux (%)	Momentum Coefficient (C_μ)
Fast acting solenoid valve	0.6	26.45	0.6359
	0.8	23.11	0.4167
Single driver shock tube	0.6	0.13	0.0032
	0.8	0.12	0.0021
Multiple driver shock tube	0.6	0.16	0.0038
	0.8	0.14	0.0025

In order to have an idea of the mechanism behind the acoustic noise suppression produced by these actuators, mean velocity and phase averaged measurements both inside and outside the cavity are made for the pulsed actuator. Due to the instantaneous nature of the shock tube actuator, mean and phase averaged measurements were not meaningful. So these measurements were carried out only for the

[3]Momentum coefficient is the ratio of the momentum of air flow through the actuator exit to the momentum of air flow through the main jet

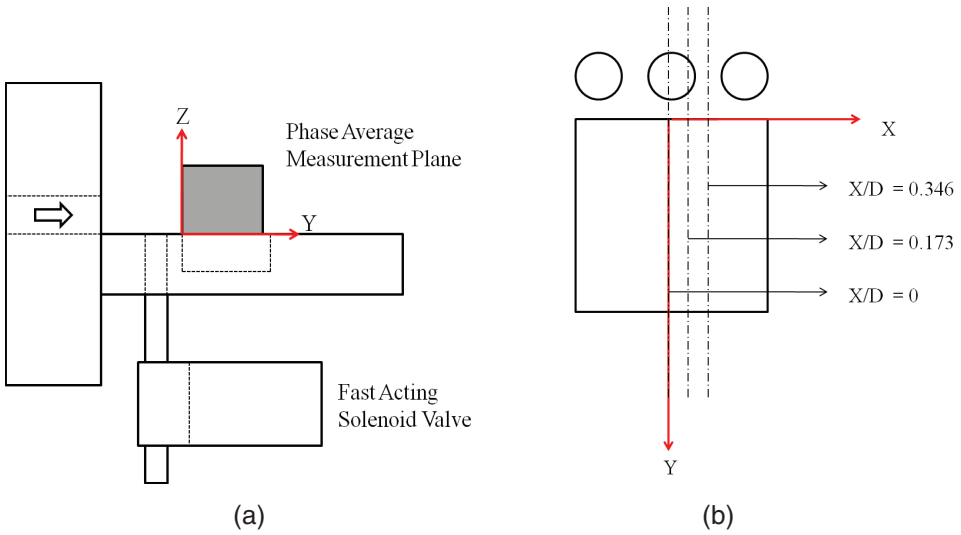

Figure 24. Schematic of the cavity noise suppression experiment using the fast acting solenoid valve indicating the planes in which the velocity and phase averaged measurements are made. (a) Side view of the setup and (b) Plan view showing the cavity and the valve exit.

steady and pulsed blowing case. The measurement plane for these measurements are shown in figure 24. The velocity measurements are taken at various points in the Y-Z plane at X/D = 0, 0.173, and 0.346 as the process is three dimensional. The axes are normalized by the depth of the cavity (D). The X/D = 0 is the center plane, X/D = 0.173 represents 1/4th the distance between the center of valve exits and finally X/D = 0.346 represents the midpoint of the distance between the center of two valve exits. The phase averaging is performed on the same plane as the velocity measurements, Y-Z plane but only at one location (X/D =0).

Let us first take a look at the velocity profile of the baseline case. Figure 25(a) shows the velocity profile taken at various downstream locations along the vertical axis at X/D = 0 for the baseline case. The spatial resolution in the Y axis was Y/D = 0.2 starting from the upstream edge of the cavity (Y/D = 0) to Y/D = 1.4. The spatial resolution in the vertical axis (Z) was Z/D = 0.1 starting from Z/D = -0.4 to Z/D = 0.6. The height of the rectangular slot jet was Z/D = 0.8. The base and roof of the jet are marked at Z/D = 0 and 0.8 respectively in the figure. The data measured at Z/D < 0 are data points inside the cavity. The experimental data points are shown in the figure as '+' and a analytical fit for the experimental data points is shown as a solid line. The spreading of the shear layer becomes evident from the figure at axial locations downstream of Y/D = 0.8 where the mean profiles indicate that the total pressure probe detects velocities at transverse locations Z/D < 0, i.e., inside the cavity. This shows the presence of air flow at the downstream edge of the cavity which indicates a strong interaction between the shear layer and the downstream edge of the cavity which is the primary reason for the generation of cavity tones. The velocity profiles at each of the downstream locations are normalized against the maximum free stream velocity such that the velocities range from 0 to 1. Figures 25(b-d) shows the velocity profile taken at various downstream locations along the vertical axis at X/D = 0, 0.173 and 0.346, respectively for the control case. The spatial resolution in the Y axis was Y/D = 0.2 starting from the upstream edge of the cavity (Y/D = 0) to Y/D = 1.4. The spatial resolution in the vertical axis (Z) was Z/D = 0.1 starting from Z/D = -0.2 to Z/D = 1.2. The first thing that we observe in all the three cases is that the velocity probe does not detect any velocity inside the cavity i.e., Z/D < 0. This indicates that there is negligible flow inside the cavity and is thus disrupting the cavity tone generation mechanism due to shear layer lift off. In figure 25(b), we observe a top-hat type of wake profile at stations close to the upstream edge of the cavity where the velocity is zero. Further downstream, the wake develops and then diffuses in the transverse direction. When comparing this result with figures 25(c,d) the effect of wake diminishes as we move from X/D = 0 to X/D = 0.346. The effect of the is more visible at X/D = 0.173 than at X/D = 0.346.

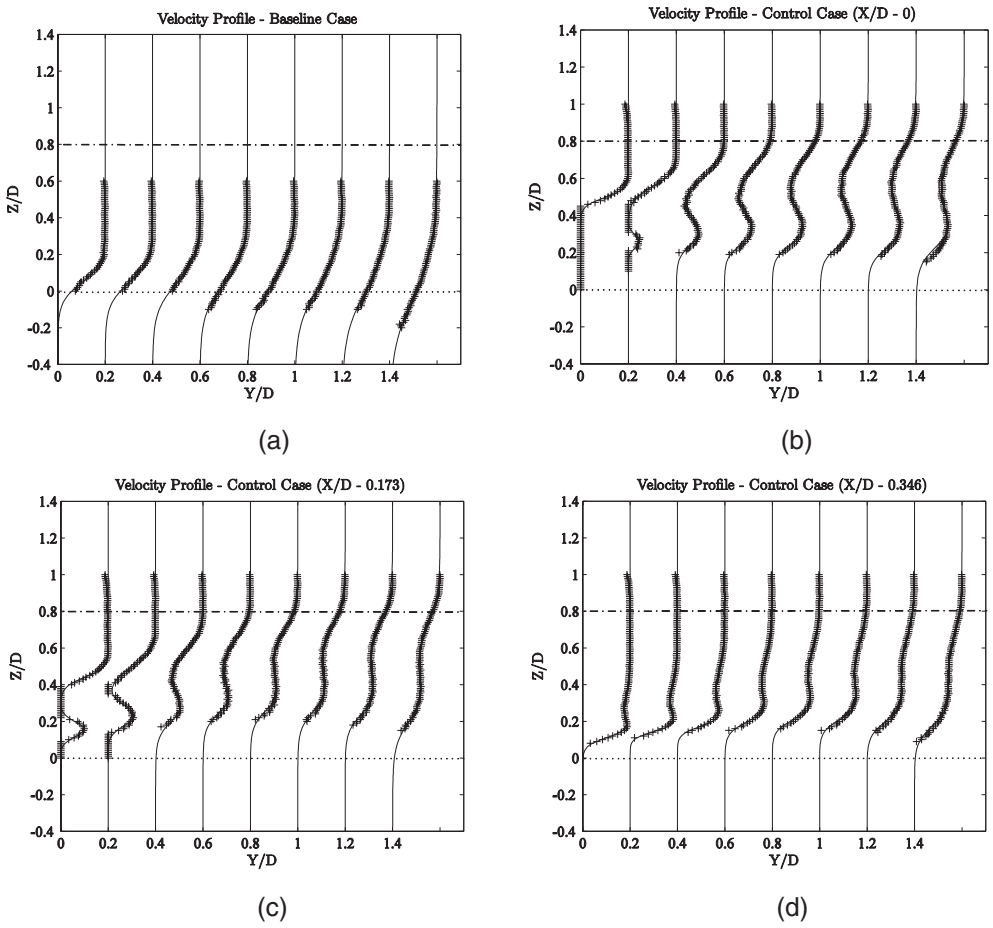

Figure 25. Distribution of the mean velocity profile of, (a) the baseline case at M 0.6, and the control case at M 0.6 on the YZ plane at (b) X/D = 0, (c) X/D = 0.173, and (d) X/D = 0.346

The phase averaged measurements were carried out with the valve pulsing at 5Hz for a free stream flow of M=0.6 over the cavity. Using the reference and measurement signals obtained from the microphone and pressure transducer, phase averaging was performed with the frequency of interest being the valve actuation frequency, i.e, 5 Hz. Figure 26 shows the phase averaged snapshots from 30^0 to 360^0 at a regular interval of 30^0. The color map indicates high and low pressure regions with red and blue color respectively. The OFF cycle of the valve ranges from 30^0 to 210^0 and the ON cycle from 210^0 to 30^0. We observe that during the OFF cycle of the valve with no air flow from the valve, there is a high pressure region close to the base indicating the presence of a jet flow passing over the cavity thus producing the cavity tone. During the ON cycle of the valve with air flow from the valves, the high pressure region near the base is replaced by a low pressure region indicating shear layer lifting due to the interaction of flow from the valves with the jet flow thus disrupting the cavity tone generation mechanism. This confirms the mechanism of shear layer lift-off observed in the velocity measurements.

4. CONCLUSION AND SUMMARY

The aim of this research work was to develop a high authority flow control actuator. We began with the idea that the miniature shock tube actuator had the potential to overcome the deficiencies of current actuator concepts. Our work consisted of two parts: (a) actuator development and (b) a demonstration experiment to assess its effectiveness. We chose cavity resonance as a flow control candidate. The main challenge was in harnessing the strength of the shock waves to disrupt the cavity tone generation mechanism. Many roadblocks were overcome in designing and developing the miniature shock tube actuators.

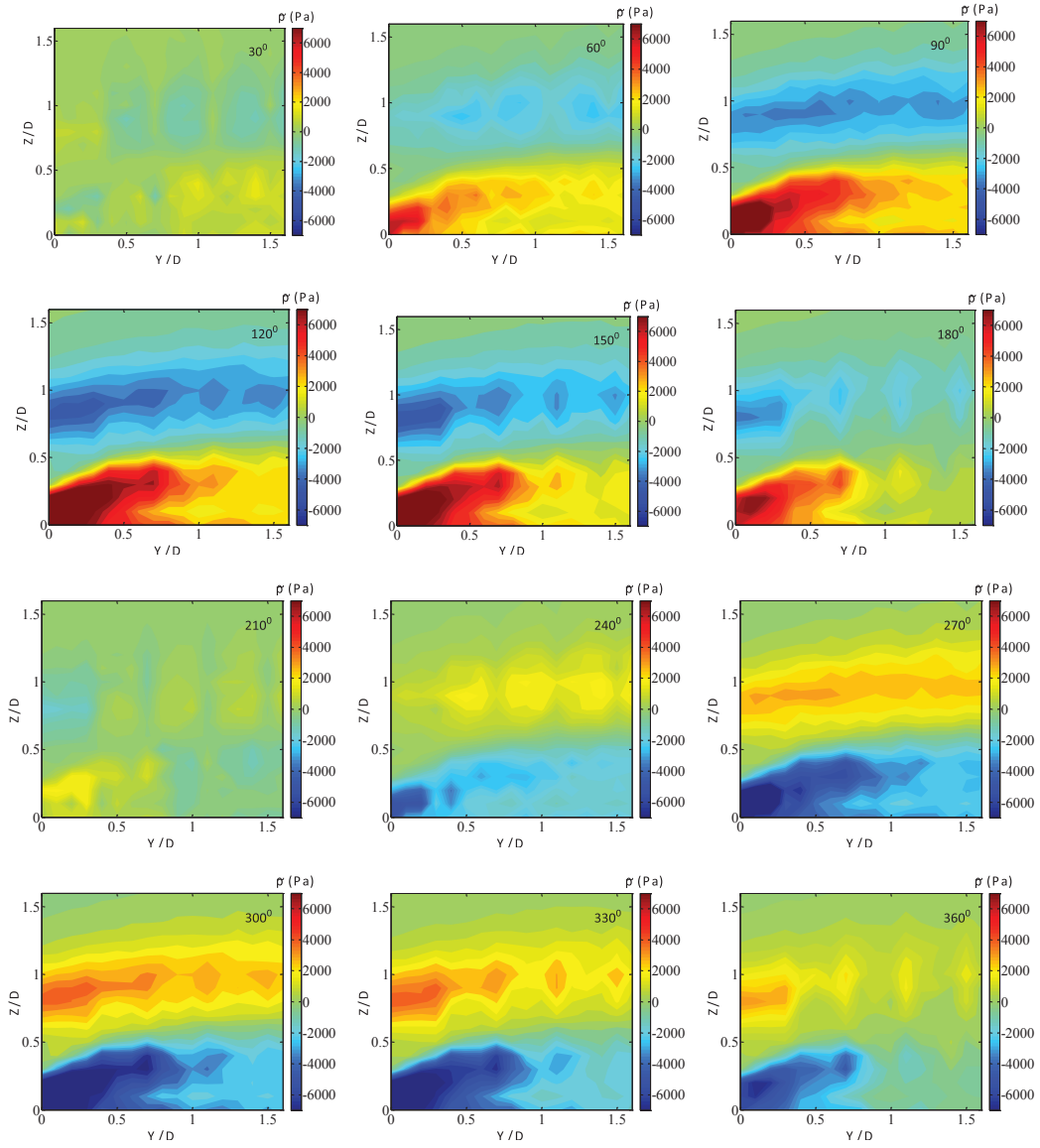

Figure 26. Phase averaged pressure measurement snapshots from phase angle 300 to 3600 at a regular interval of 300. The sequence begins from the first row and continues left to right.

The characterization experiments of the shock tube revealed that the miniature shock tubes indeed produced shock waves as predicted by theoretical equations. Unsteady pressure measurements at the exit of the single driver shock tube indicated the structure of the shock wave which included the initial shock wave followed by a constant pressure region across the contact discontinuity and then the flow behind the expansion fan. This was very much similar to the 1D shock wave theory. The experimental shock wave velocity that was measured was very close to the theoretical shock wave velocity. The experiments which involved the study of the propagation of the shock wave along the expansion chamber, revealed the presence of the reflected expansion fan from the open end of the shock tube as explained in 1-D theory. It was also observed that the closed end shock tube produced multiple reflected shock waves from the closed end which led to a series of complex flow patterns. All these results indicated that the shock waves that were generated by this miniature version of the shock tube was very much comparable to the ones predicted by theory. In order to make the shock waves more effective, a distributed shock tube approach was tested where the area of the shock tube exit was roughly

maintained the same as the single driver but three shock tubes of smaller diameter were used instead of one. Unsteady pressure measurements at the exit of such multiple driver shock tubes indicated the presence of shock waves similar to that of the single driver shock tube at the exit of all the shock tubes. There was however a small time lag between the shock waves at the exit of these shock tubes which was due to the non-uniformity in the aluminum foil diaphragm used. Upon repeating the experiments it was concluded that the time delay was random and varied with each trial. In order to compare the effect of shock tubes with that of mass injection, both steady and pulsed, fast acting solenoid valves were employed with the same exit area as the multiple driver shock tubes. The unsteady pressure measurements at the exit of these valves indicated no presence of shock waves. An ON-OFF type behavior was observed at the exit of these valves for low pulsing frequencies which gradually transformed into a impulsive behavior with increase in the pulsing frequency. It was also observed that with increase in the pulsing frequency the pressure at the exit of the valve diminished to a very low value.

The acoustic measurements showed that the fast acting solenoid valves produced very good cavity tone suppression of about 18 - 20 dB in the M = 0.6 flow (however the mass flow requirements were very high). This suppression lasted only for the duration of the air flow at the exit of the valve. The mass flux and the momentum coefficient of these valves were very high. From the pressure time history of the microphone with the shock tube operating, we observed a significant effect of the shock waves on the cavity tone. The single driver shock tube produced a tonal noise suppression of about 7 dB in M =0.6 flow whereas only a 2 dB suppression in M = 0.8 flow. Our earlier idea of spreading the shock tubes over the span of the cavity width using the multiple driver shock tube actuator showed positive results. The multiple driver shock tube produced a suppression of about 12 dB in the M = 0.6 flow and about 10 dB in the M = 0.8 flow. Upon repeating the experiments the effect of the shock wave was observed every time and produced what is known as a ‘memory effect’. The mass flux and momentum coefficients based on the duty cycle of the shock waves was found to be very low. When the diaphragm was replaced by the solenoid ON/OFF valve the velocity measurements along the downstream locations of the cavity on three different planes indicated that there is negligible flow of air inside the cavity when the valve is in its ON cycle. This suggests the lifting of the shear layer. These results were again confirmed by the phase averaged pressure measurements. The phase averaged snapshots at regular intervals of phase angles indicated the continuous lifting and amplification of the shear layer due to the ON-OFF cycle of the valve.

ACKNOWLEDGEMENTS

This work was partially funded by Jacobs/Air Force Research Lab (AFRL), Wright Patterson AFB, OH. The authors thank Dr. Michael Stanek and Mr. Rudy Johnson for their involvement in this project.

REFERENCE

[1] R. C. Ramachandran, G. Raman, J. Subburaj and G. Jagadeesh, “Miniature Shock Tube Actuators for Flow Control Applications,” in *48th Aerospace Sciences Meeting, AIAA 2010-1259*, Orlando, FL, 2010.

[2] J. Subburaj, G. Jagadeesh, R. C. Ramachandran and G. Raman, “Micro-Shock Tube Actuators for High Speed Air Vehicle Applications,” in *48th AIAA Aerospace Sciences Meeting, AIAA 2010-1201*, Orlando, FL, 2010.

[3] G. Raman, “Supersonic jet screech: half-century from Powell to the present.,” *Journal of Sound and Vibration,* vol. 214, p. 67, 1999.

[4] C. K. M. Tam and K. K. Auhja, “Theoretical model of discrete tone generation by impinging jets,” *Journal of Fluid Mechanics,* vol. 214, p. 67, 1990.

[5] D. G. Crighton, “The jet edge-tone feedback cycle- linear theory for the operating stages,” *Journal of Fluid Mechanics,* vol. 391, p. 234, 1992.

[6] M. S. Howe, “Edge, cavity and aperture tones at very low Mach numbers,” *Journal of Fluid Mechanics,* vol. 330, p. 24, 1997.

[7] L. F. East, “Aerodynamically induced resonance in rectangular cavities,” *Journal of Sound and Vibration,* vol. 3, p. 277, 1966.

[8] A. Powell, “On the edge tone,” *The Journal of the Acoustical Society of America,* vol. 33, p. 395, 1961.

[9] J. E. Rossiter, "Wind-tunnel experiments on the flow over rectangular cavities at subsonic and transonic speeds," *Aeronautical Research Council Reports and Memoranda,* vol. 8, p. 343, 1964.

[10] H. H. Heller, D. G. Holmes and E. E. Covert, "Flow induced pressure oscillations in shallow cavities.," *Journal of Sound and Vibration,* vol. 18, p. 545, 1970.

[11] L. N. Cattafesta, D. R. Williams, C. W. Rowley and F. Alvi, "Review of active control of flow-induced cavity resonance," *AIAA Paper 3567:2003,* 2003.

[12] C. W. Rowley, D. R. Williams, T. Colonius, M. Murray and D. G. MacMynowski, "Linear models for control of cavity flow oscillations," *Journal of Fluid Mechanics,* vol. 547, p. 317, 2006.

[13] S. McGrath and L. Shaw, "Active control of shallow cavity acoustic resonance," *AIAA paper, 1949:1996,* 1996.

[14] M. J. Stanek, G. Raman, V. Kibens, J. A. Ross, J. Odera and J. W. Peto, "Suppression of cavity resonance using high frequency forcing," *AIAA paper, 2128:2001,* 2001.

[15] M. J. Stanek, G. Raman, J. A. Ross, J. Odera, J. W. Peto, F. Alvi and V. Kibens, "High frequency acoustic Suppression-The role of mass flow, the notion of superposition, and the role of inviscid Instability; A new model (Part II)," *AIAA paper, 2404:2002,* 2002.

[16] M. J. Stanek, J. A. Ross, J. Odedra and J. W. Peto, "High frequency acoustic suppression- the mystery of the rod-in-crossflow revealed.," *AIAA paper, 2404:2002,* 2002.

[17] M. Bastrzyk, Cavity noise suppression through shear layer liftoff, Chicago: MS thesis, Illinois Institute of Technology, 2009.

[18] P. Panickar and G. Raman, "Using Linear Stability Analysis as a Tool to Evaluate Jet and Cavity Flow Control Situations," *International Journal of Flow Control,* vol. 1, p. 43, 2009.

[19] S. Sarpotdar, P. Panickar and G. Raman, "Linear Stability of a Hybrid Mean Velocity Profile and its Relevance to Cavity Resonance Suppression," *Physics of Fluids,* vol. 22, p. 43, 2010.

[20] G. Raman, V. Kibens, A. Cain and J. Lepicovsky, "Advanced Actuator Concepts for Active Aeroacoustic Control," *AIAA paper 2000-1930,* 2000.

[21] G. Raman and K. Srinivasan, "The powered resonance tube: From Hartmann's discovery to current active flow control applications," *Progress in Aerospace Sciences,* vol. 45, pp. 97-123, 2009.

[22] G. Raman, "Using Controlled Unsteady Fluid Mass Addition to Enhance Jet Mixing," *AIAA Journal,* vol. 35, no. 4, pp. 647-656, 1997.

[23] G. Raman and A. B. Cain, "Innovative actuators for active flow and noise control," *Journal of Aerospace Engineering,* vol. 216, pp. 303-324, 2002.

[24] A. B. Cain, E. J. Kerschen and G. Raman, "Simulation of powered resonance tube excitation of a boundary layer," in 1st *AIAA flow control conference*, AIAA 2002-2821, St. Louis, June 2002.

[25] R. Courant and K. O. Fredrichs, Supersonic Flow and Shock Waves, New York: Interscience, 1948.

[26] G. Rudinger, Wave Diagrams for Non Steady Flow in Ducts, New York: Van Nostrand, 1955.

[27] J. K. Wright, Shock Tubes, New York: John Wiely & Sons Inc., 1961.

[28] J. N. Bradley, Shock Waves in Chemistry and Physiscs, New York: John Wiley & Sons Inc., 1962.

[29] M. O. Sun and K. Takayama, "Shock propagation in narrow channels," in *22nd International Symposium on Shock Waves*, 2001.

[30] K. Ohashi and K. Takayama, "Characteristics of blast waves generated by milligram charges," in *22nd International Symposium on Shock Waves*, 2001.

[31] D. D. Dlott, "Nanoshocks in molecular materials," *Accounts of Chemical Research,* vol. 45, p. 33, 2000.

[32] G. Jagadeesh and J. Kawagishi, "A new micro-particle delivery system using laser ablation," in *22nd International Symposium on Shock Waves*, 2001.